Original Article

JCBFM

Journal of Cerebral Blood Flow & Metabolism
2018, Vol. 38(11) 2041–2052

DOI: 10.1177/0271678X17724947
journals.sagepub.com/home/jcbfm
SAGE

Kinetic evaluation and test–retest reproducibility of [^{11}C]UCB-J, a novel radioligand for positron emission tomography imaging of synaptic vesicle glycoprotein 2A in humans

Sjoerd J Finnema[1], Nabeel B Nabulsi[1], Joël Mercier[2], Shu-fei Lin[1], Ming-Kai Chen[1], David Matuskey[1], Jean-Dominique Gallezot[1], Shannan Henry[1], Jonas Hannestad[2], Yiyun Huang[1] and Richard E Carson[1,3]

Abstract

Synaptic vesicle glycoprotein 2A (SV2A) is ubiquitously present in presynaptic terminals. Here we report kinetic modeling and test–retest reproducibility assessment of the SV2A positron emission tomography (PET) radioligand [^{11}C]UCB-J in humans. Five volunteers were examined twice on the HRRT after bolus injection of [^{11}C]UCB-J. Arterial blood samples were collected for measurements of radiometabolites and free fraction. Regional time–activity curves were analyzed with 1-tissue (1T) and 2-tissue (2T) compartment models to estimate volumes of distribution (V_T). Parametric maps were generated using the 1T model. [^{11}C]UCB-J metabolized fairly quickly, with parent fraction of $36 \pm 13\%$ at 15 min after injection. Plasma free fraction was $32 \pm 1\%$. Regional time–activity curves displayed rapid kinetics and were well described by the 1T model, except for the cerebellum and hippocampus. V_T values estimated with the 2T model were similar to 1T values. Parametric maps were of high quality and V_T values correlated well with time activity curve (TAC)-based estimates. Shortening of acquisition time from 120 min to 60 min had a negligible effect on V_T values. The mean absolute test–retest reproducibility for V_T was 3–9% across regions. In conclusion, [^{11}C]UCB-J exhibited excellent PET tracer characteristics and has potential as a general purpose tool for measuring synaptic density in neurodegenerative disorders.

Keywords

Brain imaging, kinetic modeling, neurodegeneration, positron emission tomography, synapses/dendrites

Received 11 December 2016; Revised 7 July 2017; Accepted 9 July 2017

Introduction

Synaptic vesicle glycoprotein 2 (SV2) constitutes a conserved protein family in vertebrates, and is an integral membrane protein located in presynaptic vesicle membranes.[1] SV2 is vital for normal synaptic function, and plays a role in neurotransmitter release.[2] Three SV2 isoforms have been characterized, with SV2A as the only isoform distributed throughout the whole brain.[3,4] SV2A has been demonstrated to be the molecular target of the antiepileptic drug levetiracetam and the density of SV2A is reduced in the seizure onset zone in temporal lobe epilepsy patients.[5–7]

Synaptic vesicles proteins, such as SV2A, have previously been established as histologic markers of synaptic density.[8–10] The location of synaptic vesicles in

[1]Department of Radiology and Biomedical Imaging, Yale Positron Emission Tomography Center, Yale University, New Haven, CT, USA
[2]UCB Pharma, B-1420 Braine-l'Alleud, Belgium
[3]Department of Biomedical Engineering, Yale University, New Haven, CT, USA

Corresponding author:
Sjoerd J Finnema, PET Center, Yale University, 801 Howard Avenue, PO Box 208048, New Haven 06520-8048, CT, USA.
Email: sjoerd.finnema@yale.edu

brain is restricted to synaptic boutons and SV2A is ubiquitously and homogeneously present in synaptic vesicles.[3] SV2 is the vesicle protein with the least variation in the number of copies per vesicle, i.e. most "monodispersed", and this vesicle homogeneity makes SV2A a promising candidate for quantification of synaptic density.[11] Quantification of SV2A as a synaptic marker has recently been demonstrated in a mouse model of Alzheimer's disease in which Src family kinase inhibitor AZD0530 rescued both memory and synapse (SV2A) loss.[12] Thus, quantification of SV2A in the living brain has the potential to be an excellent *in vivo* proxy of synaptic density.

A number of SV2A PET radioligands have recently been reported, including [^{11}C]levetiracetam, [^{11}C]UCB-A, [^{18}F]UCB-H and [^{11}C]UCB-J.[13–16] Radiolabeling of levetiracetam itself is feasible, but the SV2A affinity of levetiracetam ($K_i = 1.6\,\mu M$) is likely too low for it to be a useful PET radioligand, and no *in vivo* evaluation has been reported so far.[15,17] The binding of [^{11}C]UCB-A in the brain of rats and pigs was found to be SV2A-specific, but binding kinetics were slow in both species, possibly related to slow metabolism and slow excretion of the tracer.[13] Binding kinetics of [^{18}F]UCB-H were promising in rats and nonhuman primates, [^{18}F]UCB-H has acceptable dosimetry in rats and humans, and a simpler synthetic route has recently been described, but an *in vivo* brain quantification study has not yet been reported.[16,18–21] Also, in nonhuman primates, [^{11}C]UCB-J had higher SV2A specific binding than [^{18}F]UCB-H.[14]

We previously reported the development of [^{11}C]UCB-J ((*R*)-1-((3-[^{11}C]methylpyridin-4-yl)methyl)-4-(3,4,5-trifluorophenyl)pyrrolidin-2-one).[14] [^{11}C]UCB-J exhibited excellent characteristics as an SV2A PET radioligand in nonhuman primates, including high brain uptake and fast kinetics. Pretreatment studies with levetiracetam and displacement studies with brivaracetam confirmed specific binding to SV2A.[22] More recently, we demonstrated in a baboon PET-postmortem study that SV2A is a valid alternative synaptic density marker to synaptophysin.[23] Initial first-in-human PET studies demonstrated that [^{11}C]UCB-J had high brain uptake and fast kinetics in humans and that [^{11}C]UCB-J binding could be displaced by levetiracetam.[23] Most importantly, large local changes in [^{11}C]UCB-J medial temporal lobe binding were shown in patients with temporal lobe epilepsy.[23]

To further validate the use of [^{11}C]UCB-J in clinical studies, we here performed a kinetic evaluation of [^{11}C]UCB-J in human volunteers. Five healthy subjects were examined twice with [^{11}C]UCB-J to assess the reproducibility of [^{11}C]UCB-J pharmacokinetic and binding parameters between the test and retest PET measurements.

Materials and methods

Human volunteers

Five volunteers participated in the study (four men and one woman; age: 37 ± 13 years, range: 25–55 years; weight: 83 ± 18 kg, range: 58–108 kg). The subjects are the same as in a previous study in which data of the initial baseline studies were included.[23] The study was performed under a protocol approved by the Yale University Human Investigation Committee and the Yale New Haven Hospital Radiation Safety Committee, and in accordance with the United States federal policy for the protection of human research subjects contained in Title 45 Part 46 of the Code of Federal Regulations (45 CFR 46). Written informed consent was obtained from all participants after complete explanation of study procedures.

Radiotracer synthesis

[^{11}C]UCB-J was synthesized according to previously described procedures.[14]

PET imaging experiments

All subjects underwent two [^{11}C]UCB-J PET measurements on the same day. The time between injections was 4.9 ± 1.6 h, range: 2.9–7.2 h. Subjects were allowed to consume a light lunch during the interval between the two PET measurements. PET scans were conducted on the High Resolution Research Tomograph (HRRT; Siemens, Medical Solutions, Knoxville, TN, USA), which acquires 207 slices (1.2 mm slice separation) with a reconstructed image resolution (FWHM) of ~3 mm. Before every [^{11}C]UCB-J injection, a 6-min transmission scan was performed for attenuation correction. PET data were acquired in list-mode for 120 min after intravenous infusion of [^{11}C]UCB-J over 1 min by an automated infusion pump (Harvard PHD 22/2000; Harvard Apparatus, Holliston, MA, USA). The injected mass was limited to 10 μg of UCB-J and 1 μg of other UV components per injection. The dynamic emission data were reconstructed into 33 frames (6×0.5 min, 3×1 min, 2×2 min, and 22×5 min) with corrections for attenuation, normalization, scatter, randoms, and dead time using the MOLAR algorithm.[24] Event-by-event motion correction was included in the reconstruction based on motion detection with a Polaris Vicra® optical tracking system (NDI Systems, Waterloo, Canada) using reflectors mounted on a swim cap worn by the subject.[25]

Blood analyses

All subjects underwent arterial cannulation and blood was collected for measurement of the time course of [^{11}C]UCB-J in plasma, including radiometabolite analysis. Samples were drawn every 10 s for the first 90 s and at 1.75, 2, 2.25, 2.5, 2.75, 3, 4, 5, 6, 8, 10, 15, 20, 25, 30, 45, 60, 75, 90, 105, and 120 min after [^{11}C]UCB-J injection. For each sample, plasma was obtained by centrifugation at 4°C (2,930 *g* for 5 min). Whole blood and plasma samples were counted in cross-calibrated gamma-counters (1480 Wizard; Perkin-Elmer, Waltham, MA, USA). The tail of the blood and plasma radioactivity curves was fitted to a sum of exponentials to reduce noise in the input function.

Radiometabolite analyses were performed for plasma samples at 3, 8, 15, 30, 60, and 90 min using an automatic column-switching HPLC system as described in our previous publication.[26,27] All HPLC eluate was fraction-collected and counted in the gamma-counters (2480 Wizard; Perkin-Elmer, Waltham, MA, USA). The sample recovery rate, extraction efficiency, and HPLC fraction recovery were monitored by measuring radioactivity in the plasma, plasma filter, plasma filtrate, and HPLC fractions. The unmetabolized parent fraction was determined as the ratio of the radioactivity corresponding to the parent to the total amount of radioactivity collected and fitted with an inverted integrated gamma function. The curve was normalized with the time-varying extraction efficiency, which was determined by corresponding reference plasma samples and fitted with an exponential function. The arterial plasma input function was calculated as the product of the total plasma activity, the [^{11}C]UCB-J HPLC fraction curve, and the extraction efficiency curve.[27] The HPLC method was optimized to allow for proper separation of three radiometabolite fractions in plasma during the PET measurements in volunteers 1 and 2. Radiometabolite fractions were quantified in volunteers 3–5. All peaks present in the radiochromatogram were integrated and radiometabolite fractions were expressed as relative to the total area under the curve.

Plasma free fraction (f_p) was measured in triplicate using an ultrafiltration method (Millipore Centrifree® micropartition device 4104, Billerica, MA, USA) following the guidelines provided by the manufacturer with 4 mL of arterial blood sample taken immediately prior to injection. The f_p values were determined as the radioactivity ratio of ultrafiltrate to plasma.

Image analysis

T1-weighted magnetic resonance (MR) images were acquired on a 3-T whole-body scanner (Trio, Siemens Medical Solutions, Erlangen, Germany) with a circularly polarized head coil. The dimension and pixel size of MR images were $256 \times 256 \times 176$ and $0.98 \times 0.98 \times 1.0\,mm^3$, respectively. Post-processing of the MR images included skull- and muscle stripping procedures (FMRIB's Brain Extraction Tool, http://fsl.fmrib.ox.ac.uk/fsl/fslwiki/BET) and were performed to obtain "brain tissue only" images for coregistration with the PET images and the template MRI.

Image registration and definition of regions of interest

An average PET image (mean of the frames corresponding to 0–10 min) was aligned to each subject's MR image via a rigid registration with mutual information. The individual MR image was normalized to Montreal Neurological Institute space using an affine linear plus nonlinear registration (BioImage Suite 2.5), to extract regions-of-interest (ROIs) from the automated anatomic labeling (AAL) template.[28,29] Regional time–activity curves were obtained by applying the template ROIs to PET space using the inverse of the two image-transformations (i.e. PET-to-MRI and MR-to-template). The following AAL regions were included: amygdala, anterior cingulate cortex, caudate nucleus, cerebellum, frontal cortex, globus pallidus, hippocampus, insular cortex, occipital cortex, parietal cortex, posterior cingulate cortex, putamen, temporal cortex and thalamus. The ROI for the centrum semiovale was based on the AAL region but was eroded by two voxels on all borders to minimize partial volume effects.

Quantitative analysis

Kinetic analysis was performed with the regional TACs using the metabolite-corrected arterial plasma TAC as an input function. The outcome measure distribution volume (V_T) was calculated with the 1-tissue compartment model (1T) and 2-tissue compartment model (2T). The time delay was determined globally by adding this parameter to the 1T model and fitting the first 10 min of the whole-brain TAC; this value was fixed in all subsequent fits. To evaluate the effect of a blood volume term in the model, blood volume fraction was fit or fixed to 0.05. The relative performance of 1T and 2T models was based on the Akaike Information Criterion (AIC), F tests, and comparison of V_T and K_1 values and their reproducibility. The AIC was calculated as follow

$$AIC = N \times \ln(SumSQ/N) + 2 \times k$$

Here N is the number of fitted frames, and k is the number of fitted parameters. For parameter estimation, data points were weighted based on the noise equivalent counts in each frame.[30] Percentage standard error (%SE) was estimated from the theoretical parameter covariance matrix. Comparison of K_1, V_T and V_T/f_p values calculated by different models was limited to the values which were reliably estimated, e.g. with a %SE less than 25%. Parametric images for the 1T model were created with a basis function method with k_2 limited to the range ($0.01–1.0\,min^{-1}$) and with no post-smoothing. All modeling was performed with in-house programs written within IDL 8.0 (ITT Visual Information Solutions, Boulder, CO, USA).

The time-stability of V_T values was evaluated by fitting the regional TACs for PET data with truncated acquisition times, ranging from 120 to 20 min. The ratio of regional V_T value from the truncated scan to that from the 120 min measurement was computed for each ROI. Minimum acceptable acquisition time was assessed for each region according the following two criteria: (1) the average V_T ratio was between 95 and 105%; (2) the interindividual standard deviation of the ratio was lower than 10%.

The reproducibility of the obtained outcome parameters was examined by calculation of the relative test–retest variability (TRV) and the absolute TRV (aTRV). The TRV and aTRV were calculated as following:

$$TRV = \frac{retest\ value - test\ value}{(test\ value + retest\ value)} \times 200\%$$

$$aTRV = \frac{|retest\ value - test\ value|}{(test\ value + retest\ value)} \times 200\%$$

To evaluate within-subject variability relative to between-subject variability, intraclass correlation coefficient (ICC) values were calculated for each region as following:

$$ICC = \frac{(BSMSS - WSMSS)}{(BSMSS + WSMSS)}$$

Here BSMSS indicates the between-subject mean sum of squares and WSMSS indicates the within-subject mean sum of squares. ICC can vary from -1 (no reliability) to $+1$ (perfect reliability).

Statistical analysis between test and retest conditions was performed with two-tailed, paired t-tests with $P < 0.05$. A Bonferroni correction was used to correct for multiple comparisons in the laterality examination (12 regions, excluded were anterior cingulate cortex, centrum semiovale and posterior cingulate cortex). All data are presented as mean ± standard deviation (SD).

Results

Injection parameters

The radiochemical purity of [^{11}C]UCB-J was over 99%. The injected radioactivity of [^{11}C]UCB-J was 544 ± 145 MBq (range: 306–702 MBq) for the test PET measurements and 538 ± 150 MBq (range: 358–715 MBq) for the retest PET measurements. The specific radioactivity at the time of injection was 107 ± 21 GBq/μmol (range: 74–132 GBq/μmol) for the test PET measurements and 135 ± 44 GBq/μmol (range: 88–193 GBq/μmol) for the retest PET measurements. The corresponding mean injected mass dose of UCB-J was 1.65 ± 0.30 μg (range: 1.34–2.08 μg) and 1.38 ± 0.46 μg (range: 0.71–1.93 μg) for the test and retest PET measurements, respectively. There were no statistical significant differences between the test and retest condition in the injected amount of radioactivity, specific radioactivity, or injected mass dose. The mean injected mass dose of UCB-J was 19 ± 5 ng/kg and expected to induce <1% SV2A occupancy based on the *in vivo* affinity of UCB-J previously determined as 3.4 nM (~20 μg/kg) in nonhuman primates.[14] Thus, there is no likelihood of carryover effects between the two injections.

Blood analysis

The mean extraction efficiency and HPLC fraction recovery value were >97% at all time points. Representative HPLC radiochromatograms from plasma samples obtained at 3, 8, 15, 30, 60 and 90 after injection of [^{11}C]UCB-J in volunteer 3 are displayed in Figure 1(a). After injection of [^{11}C]UCB-J, three radiometabolite fractions were detected during the course of the PET measurement. The three radiometabolite fractions had a retention time of 6.4 ([^{11}C]M0), 6.9 ([^{11}C]M1) and 7.7 ([^{11}C]M2) min, respectively, eluting earlier than [^{11}C]UCB-J (10.5 min). Figure 1(b) to (d) displays the average of the total radioactivity concentration in plasma, the parent and radiometabolite fractions, and the parent plasma concentration over the time course of the test and retest PET measurements, respectively. The [^{11}C]UCB-J fraction in plasma was slightly smaller in the retest condition (Figure 1(c)), with a statistical significant difference of 10 ± 6.7% at 8 min. There was no significant difference in the integral of the [^{11}C]UCB-J plasma concentration (Figure 1(d)). The f_p of [^{11}C]UCB-J was 0.32 ± 0.007 (range: 0.32–0.33) for the test and 0.32 ± 0.019 (range: 0.29–0.34) for the retest PET measurement ($P = 0.90$), respectively. The TRV of f_P was 0 ± 6% and the aTRV was 4 ± 4%.

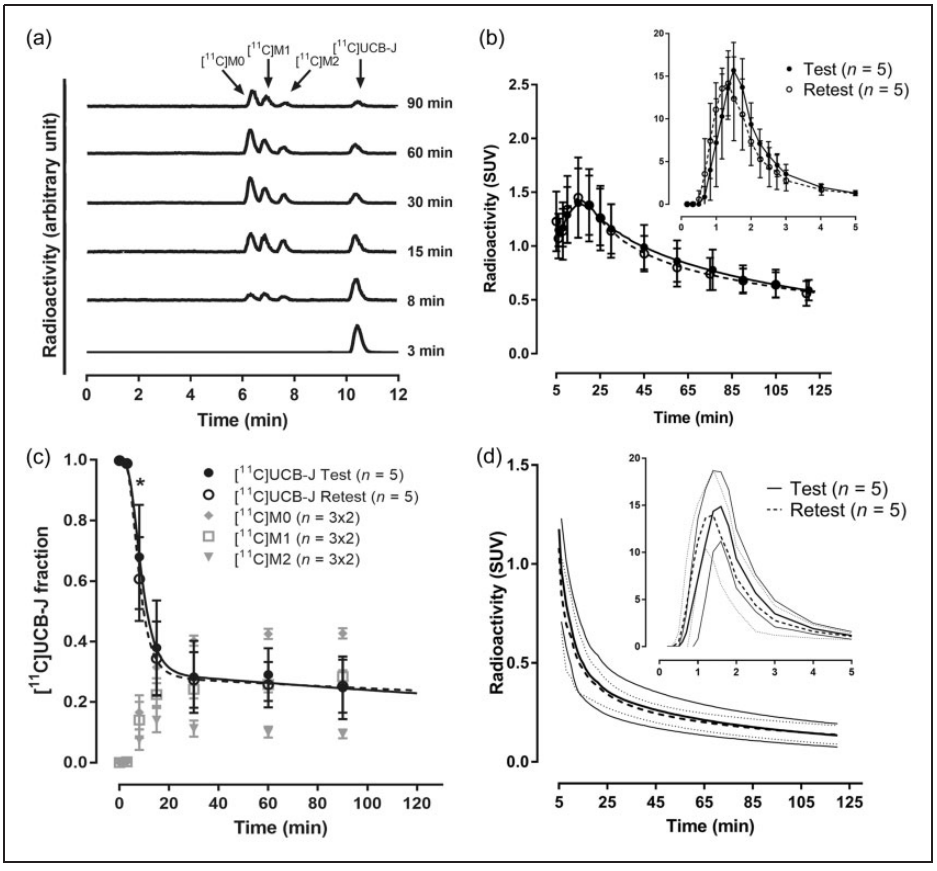

Figure 1. Radioactivity content in plasma after intravenous injection of [^{11}C]UCB-J in human. (a) HPLC radiochromatograms of plasma content 3, 8, 15, 30, 60 and 90 min after [^{11}C]UCB-J injection in volunteer 3 during test condition. (b) Total plasma radioactivity concentration over time (data are mean ± SD). (c) Unchanged [^{11}C]UCB-J and radiometabolite fractions in plasma over time (data are mean ± SD). (d) [^{11}C]UCB-J concentration in plasma over time (data are mean, 95% confidence interval is indicated with solid line for test and with dotted line for retest condition). *$P < 0.05$.
SUV: standard uptake value.

Quantification of [^{11}C]UCB-J binding

After injection of [^{11}C]UCB-J, there was a rapid uptake of radioactivity in the brain, with high radioactivity concentrations in gray matter regions and low concentrations in white matter regions (Figures 2 and 3). The peak standardized uptake value was 6–12 across the gray matter brain regions, and was achieved 10–25 min after [^{11}C]UCB-J injection. The uptake in the white matter region, centrum semiovale, was considerably lower than in all examined gray matter regions. A steady decline in regional radioactivity over time was observed starting approximately 20 min after injection.

Evaluation of the fitting of the regional TACs was initiated with determining the time delay between the arrival of radioligand in the brain and radial artery blood samples. The estimated delay was 20 ± 4 s, (range: 15–25 s, $n = 5$) and 14 ± 5 s, (range: 8–19 s, $n = 5$) for the test and retest PET measurement ($P = 0.11$), respectively. Inclusion of the blood volume fraction into the 1T fit decreased the delay from 17 ± 5 sec to 8 ± 5 s with a fixed blood volume of 5%, and to 5 ± 3 s with free fit of blood volume fraction.

However, inclusion of the blood volume fraction into the 1T or 2T model fit did not affect the regional K_1 or V_T values (Supplemental Figures 1 and 2). The aTRV of K_1 and V_T values was also not improved when including the blood volume fraction (data not shown). This result is consistent with the much lower plasma radioactivity concentration (Figure 1(b)) than brain radioactivity concentration (Figure 3). Therefore, the blood volume fraction was excluded from the kinetic evaluation.

The 1T and 2T models reached convergence in all evaluated regional TACs (Figure 3). The mean K_1 value estimated with the 1T model ($n = 10$, Table 1) ranged from 0.129 ± 0.014 mL/cm^3 per minute in the centrum semiovale to 0.387 ± 0.048 mL/cm^3 per minute in the putamen. The mean value of V_T in the 1T model

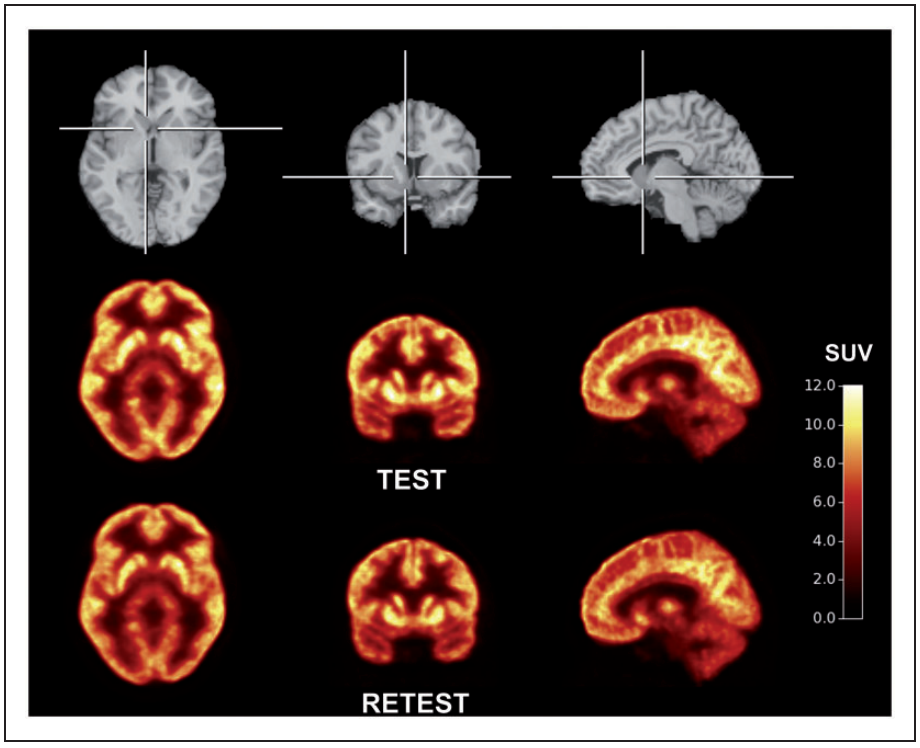

Figure 2. Template MR images (top) and aligned PET images of [^{11}C]UCB-J during test (middle) and retest (bottom) condition. PET summation images (average of frames from 40 to 60 min) represent the mean of five subjects.

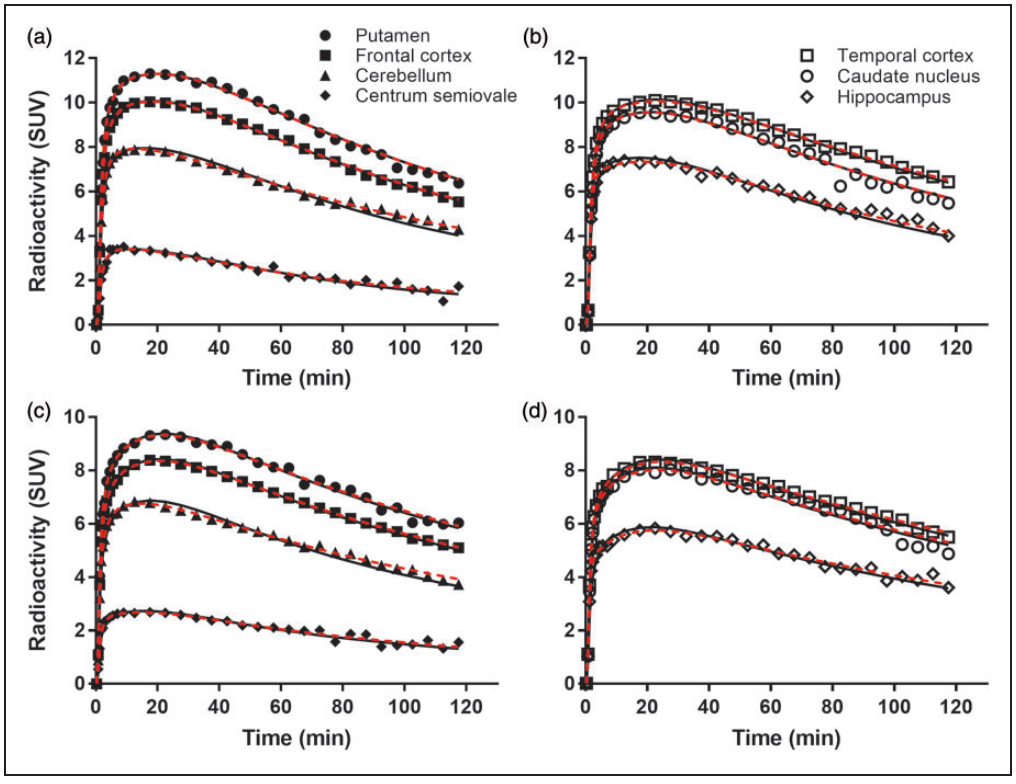

Figure 3. Time course for regional brain radioactivity and curve fitting with the 1T (black solid line) and 2T (red dotted line) model in volunteer 1 during (a and b) test and (c and d) retest condition.
SUV: standard uptake value.

Table 1. Kinetic parameters of [^{11}C]UCB-J under test and retest condition derived with 1T model from 120 min TACs.

	K_1 (mL/cm^3 per min)			V_T (mL/cm^3)			V_T/f_p (mL/cm^3)		
Region	All	Test	Retest	All	Test	Retest	All	Test	Retest
Putamen	0.387 (12)	0.383 (12)	0.391 (14)	22.4 (8)	22.4 (9)	22.4 (7)	70 (6)	70 (8)	69 (5)
Temporal cortex	0.333 (10)	0.330 (12)	0.337 (10)	21.0 (9)	21.1 (10)	20.9 (9)	65 (7)	66 (9)	65 (5)
Insular cortex	0.336 (12)	0.342 (13)	0.330 (13)	20.8 (8)	20.9 (10)	20.6 (7)	64 (6)	65 (8)	64 (5)
Ant. cingulate cortex	0.333 (13)	0.333 (14)	0.333 (15)	20.5 (8)	20.5 (8)	20.6 (9)	64 (6)	64 (7)	64 (5)
Amygdala	0.237 (14)	0.242 (18)	0.232 (11)	19.6 (9)	19.8 (11)	19.3 (7)	61 (9)	62 (10)	60 (9)
Parietal cortex	0.348 (11)	0.350 (10)	0.347 (13)	19.7 (11)	19.8 (12)	19.7 (11)	61 (8)	61 (11)	61 (6)
Occipital cortex	0.359 (7)	0.363 (8)	0.355 (7)	19.4 (9)	19.6 (11)	19.3 (9)	60 (7)	61 (9)	60 (6)
Caudate nucleus	0.308 (18)	0.304 (19)	0.313 (19)	18.7 (12)	18.8 (12)	18.6 (14)	58 (11)	58 (10)	58 (13)
Frontal cortex	0.354 (11)	0.350 (11)	0.358 (12)	18.8 (9)	18.7 (10)	18.8 (8)	58 (6)	58 (8)	58 (5)
Globus pallidus	0.279 (8)	0.278 (8)	0.279 (9)	15.3 (7)	15.6 (8)	15.0 (5)	47 (6)	49 (7)	46 (5)
Thalamus	0.352 (10)	0.340 (9)	0.364 (10)	15.5 (5)	15.4 (5)	15.6 (5)	48 (5)	48 (3)	48 (6)
Cerebellum	0.300 (10)	0.298 (10)	0.302 (10)	14.5 (7)	14.4 (8)	14.5 (7)	45 (5)	45 (7)	45 (5)
Hippocampus	0.237 (9)	0.238 (12)	0.235 (7)	14.2 (8)	14.2 (7)	14.1 (10)	44 (8)	44 (6)	44 (11)
Post. cingulate cortex	0.303 (12)	0.298 (14)	0.308 (11)	14.1 (15)	14.2 (16)	14.1 (16)	44 (14)	44 (15)	44 (16)
Centrum semiovale	0.129 (11)	0.130 (13)	0.128 (10)	5.3(10)	5.3 (10)	5.3 (11)	16 (8)	17 (10)	16 (7)

Note: Data are ranked in order according to V_T value. Data are mean and within parentheses are percentage coefficient of variation.
Ant.: anterior; Post.: posterior; 1T: 1-tissue compartment model; TAC: time activity curve.

ranged from 5.3 ± 0.5 mL/cm^3 in the centrum semiovale to 22.4 ± 1.8 mL/cm^3 in the putamen. Corresponding regional V_T/f_p values were between 16 mL/cm^3 to 70 mL/cm^3 (Table 1). There was no evidence of laterality in the K_1, V_T or V_T/f_p values.

For model selection, comparison of the AIC values and F-test of the weighted sum of squared residuals of the 1T and 2T model fits indicated that in, respectively, 83% and 73% of the 150 fits, the 2T model was the preferred model (Supplemental Table 1). However, 6% of the K_1 values and 20% of the V_T values were not reliably estimated with the 2T model (rSE > 25%). Comparing the reliable estimates, K_1 values from the 2T model were $8 \pm 10\%$ ($n = 141$) higher than the 1T values. The mean underestimation in K_1 with 1T was largest in hippocampus ($33 \pm 15\%$), amygdala ($16 \pm 13\%$) and anterior cingulate cortex ($15 \pm 8\%$), and <10% in other regions. V_T values were in closer agreement, with 2T values being $3 \pm 3\%$ ($n = 120$) higher than 1T values. The mean underestimation in V_T with 1T was largest in cerebellum ($7 \pm 4\%$) and <5% in other regions. Bland-Altman plots were consistent with a negative bias in K_1 for 1T (Supplemental Figure 3). K_1 values were well correlated between methods: $K_1(2T) = 0.966 \times K_1(1T) + 0.0334$, $R^2 = 0.8899$, while V_T values were highly correlated between methods: $V_T(2T) = 1.018 \times V_T(1T) + 0.166$; $R^2 = 0.983$ (Supplemental Figures 4 and 5). The 1T model thus provides highly acceptable estimates of K_1 and V_T values except for the hippocampus and cerebellum, respectively.

Voxel-based parametric maps were obtained for K_1 and V_T values using the 1T model and 120 min of PET data time (Figure 4). Comparison of the K_1 and V_T values indicated that the values were, respectively, $0 \pm 1\%$ ($n = 150$) and $1 \pm 2\%$ ($n = 150$) higher from the parametric maps than for the TAC based values. Regional K_1 and V_T values from regional TAC based values agreed extremely well with values obtained using the parametric maps ($R^2 = 0.99$) (Supplemental Figure 6(a) and (b)).

Table 2 lists the TRV and aTRV results for each region for K_1, V_T and V_T/f_p obtained with the TAC-based analysis. The mean regional TRV and aTRV were $0.60 \pm 7.0\%$ and $5.7 \pm 4.1\%$ for K_1, $-0.8 \pm 5.7\%$ and $4.4 \pm 3.2\%$ for V_T, and $-1.0 \pm 8.1\%$ and $6.7 \pm 3.4\%$ for V_T/f_p, respectively. These are all excellent reproducibility values. For voxel-based analyses, the TRV characteristics were virtually identical: the regional mean TRV and aTRV were $0.4 \pm 6.9\%$ and $5.6 \pm 4.0\%$ for K_1, $-0.7 \pm 5.2\%$ and $4.2 \pm 2.6\%$ for V_T, and $-0.9 \pm 7.5\%$ and $6.3 \pm 3.0\%$ for V_T/f_p, respectively (Supplemental Table 2). ICC values were similar for TAC- and voxel-based analyses (Supplemental Table 3). The ICC for K_1 and V_T were typically above 0.6, but lower for K_1 in the occipital cortex and thalamus and lower for V_T in small regions such as amygdala and globus pallidum. ICC values for V_T/f_p

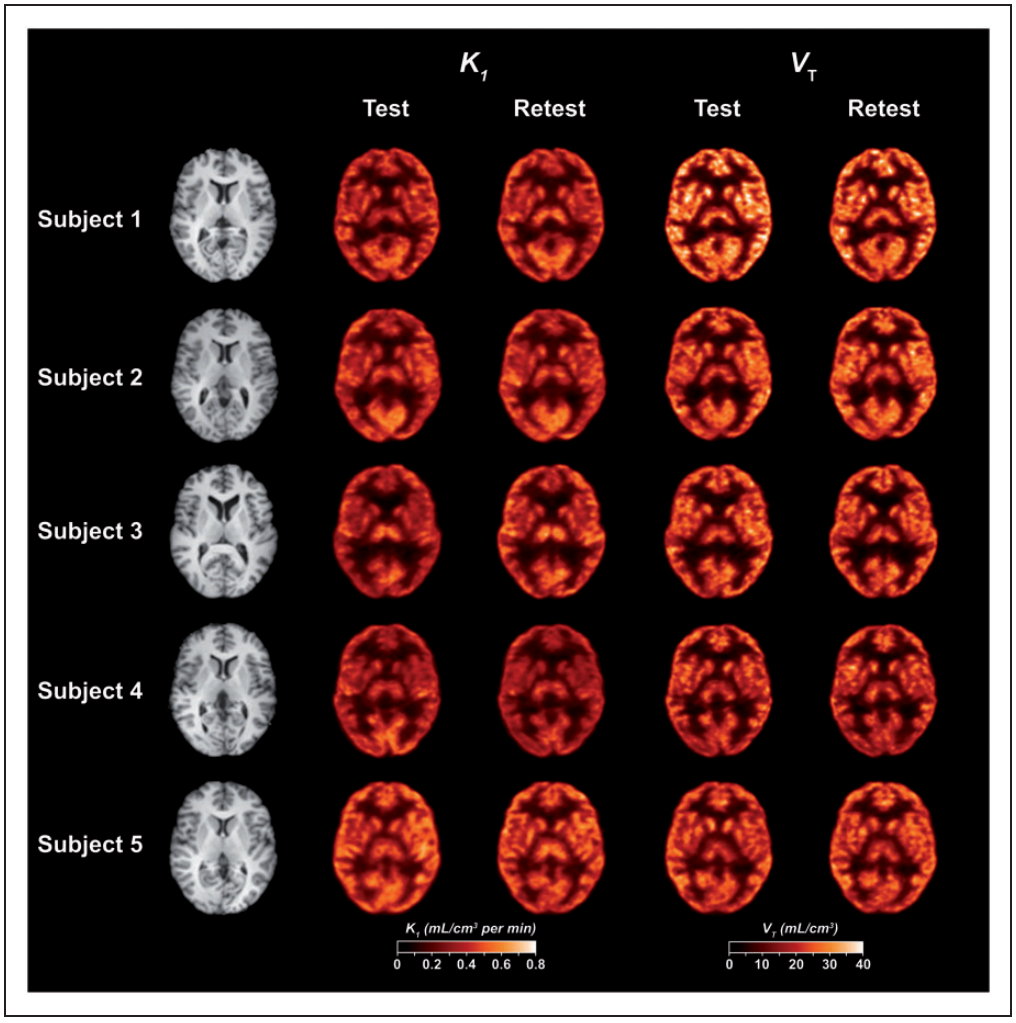

Figure 4. Individual MR images (left) and aligned parametric maps for K_1 and V_T of [^{11}C]UCB-J using 1-tissue model and 120 min of PET data time during test and retest condition.

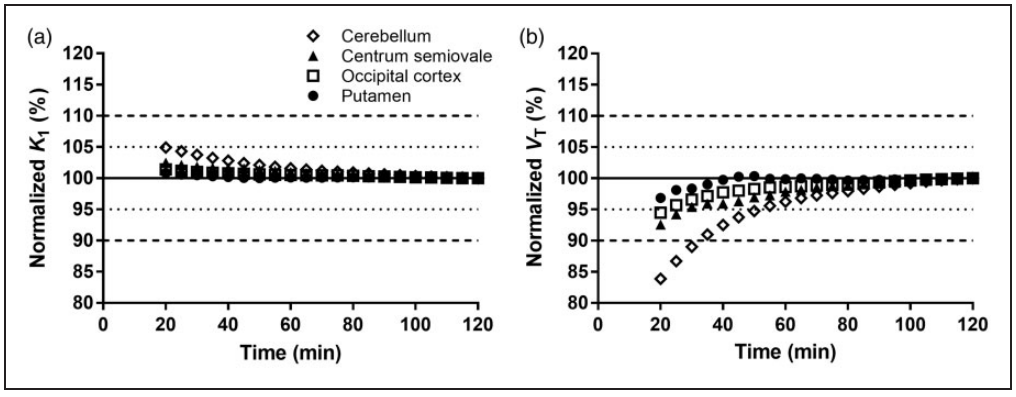

Figure 5. Time stability analyses of outcome parameters K_1 and V_T. (a) K_1 values and (b) V_T values were calculated by 1T model and divided by the value measured using 120 min of PET data time. Data are means ($n = 10$), the SD was not displayed for the sake of clarity.

Table 2. Test–retest reproducibility of kinetic parameters of [^{11}C]UCB-J derived with 1T model from 120 min of TACs.

	K_1 (mL/cm^3 per min)		V_T (mL/cm^3)		V_T/f_p (mL/cm^3)	
Region	aTRV	TRV	aTRV	TRV	aTRV	TRV
Putamen	4%	2% ± 5%	5%	0% ± 6%	7%	0% ± 9%
Temporal cortex	7%	2% ± 10%	4%	−1% ± 5%	6%	−1% ± 7%
Insular cortex	8%	−3% ± 9%	5%	−1% ± 6%	7%	−1% ± 9%
Ant. cingulate cortex	4%	0% ± 6%	5%	0% ± 6%	6%	0% ± 7%
Amygdala	9%	−3% ± 11%	9%	−2% ± 14%	12%	−3% ± 16%
Parietal cortex	5%	−1% ± 7%	4%	−1% ± 5%	5%	−1% ± 6%
Occipital cortex	8%	−2% ± 11%	4%	−1% ± 5%	5%	−2% ± 6%
Caudate nucleus	4%	3% ± 4%	4%	−1% ± 6%	7%	−1% ± 9%
Frontal cortex	4%	2% ± 7%	3%	1% ± 4%	5%	0% ± 6%
Globus pallidus	3%	0% ± 4%	7%	−4% ± 8%	9%	−4% ± 10%
Thalamus	7%	7% ± 7%	3%	2% ± 4%	6%	1% ± 7%
Cerebellum	3%	1% ± 4%	3%	1% ± 3%	6%	1% ± 7%
Hippocampus	5%	−1% ± 7%	4%	−1% ± 6%	8%	−1% ± 9%
Post. cingulate cortex	6%	3% ± 7%	3%	−1% ± 3%	6%	−1% ± 7%
Centrum semiovale	6%	−1% ± 8%	3%	−1% ± 5%	7%	−2% ± 9%

Note: Data are mean ± SD.
Ant.: anterior; aTRV: absolute test–retest variability; Post.: posterior; TRV: test–retest variability; 1T: 1-tissue compartment model; TAC: time activity curve.

were lower than 0.6 in eight of the examined brain regions.

To assess the time stability of the outcome measures, the effect of the duration of the PET data period on K_1 and V_T was estimated. The normalized K_1 and V_T values (ratio to 120-min values) are displayed in Figure 5. Overall, the K_1 and V_T values were extremely stable. Using PET data time of 60 min resulted in mean regional K_1 and V_T values of 101 ± 1% and 98 ± 3% of the terminal value. Across the 10 scans and 15 regions, at 60 min the largest difference in K_1 and V_T values was 4% and 8%, respectively. Presented in another manner, there was an excellent correlation ($R^2 > 0.99$) between the K_1 and V_T values obtained from the parametric maps using 60 min and 120 min of PET data time (Supplemental Figure 7). Importantly, the ICC, TRV, and aTRV were not reduced when using only 60 min of PET data time (Supplemental Tables 3 to 5).

Discussion

The current study included kinetic analysis and a test–retest reproducibility examination of the regional outcome parameters of [^{11}C]UCB-J, a new PET SV2A tracer. Overall, we found that [^{11}C]UCB-J has exceptional kinetic properties and is an outstanding PET radioligand for quantification of SV2A in the human brain.

Evaluation of the radioactivity content in plasma indicated the formation of at least three radiometabolites, which were all more polar than [^{11}C]UCB-J. Comparative HPLC analysis of the radioactivity content in plasma samples with chemical standards of two potential metabolites indicated that [^{11}C]M1 and [^{11}C]M2 are likely formed by *N*-oxidation and methyl hydroxylation, respectively (data not shown). Both these radiometabolites were previously shown to be present in rat plasma, but only at trace levels (<1.5%) in the rat brain.[14] The fraction of [^{11}C]M0 was small, up to 10% of plasma radioactivity at 90 min, and [^{11}C]M0 was previously not observed in rat plasma or brain, nor in human liver microsomes. We hypothesize that [^{11}C]M0 may be the product of further oxidation of [^{11}C]M1 or [^{11}C]M2, resulting in either methyl hydroxylation of the *N*-oxide or formation of the carboxylic acid, respectively. The results of these blood-based analyses were also consistent with the results of the kinetic modeling of the PET data, which indicated that the time-stability of the regional V_T values was exceptionally good. In summary, there is no evidence of a contribution of brain-penetrant radiometabolites to the PET signal in brain.

The very high brain uptake and regional distribution of [^{11}C]UCB-J was consistent with our previous *in vitro* and *in vivo* SV2A measurements in the nonhuman primate brain.[14,23] The regional distribution of SV2A in the human brain has not been described in detail by other methods than with PET.[23] Previous studies using post-mortem brain tissue included relative large areas, such as cortex, hippocampus and cerebellum.[17]

Future studies are required, e.g., with autoradiography, to allow for detailed comparison of SV2A distribution between humans and nonhuman primates.

Radioactivity concentrations were high in all gray matter regions and lowest in the centrum semiovale. By strict modeling considerations, regional TACs were best described with the 2T model. However V_T estimates were unstable in 20% of the 2T fits, mainly due to poor estimation of k_4 even when fitting 120 min of data. Overall, the 1T and 2T model provided K_1 and V_T values which were nearly identical and highly correlated. Underestimation of K_1 values in the hippocampus by 1T was not due to region-specific differences in delay or blood volume (see Supplemental Figure 2) and may have been caused by tissue heterogeneity of gray and white matter. The use of the 1T model for estimation of K_1 values in hippocampus, amygdala and anterior cingulate cortex should thus be performed with caution. However, considering that the primary outcome parameter is V_T, we chose the 1T model as most appropriate. In general, use of the 1T model will provide higher precision and ease of production of parametric images.

The test–retest reproducibility of [^{11}C]UCB-J V_T was exceptionally good, and better than we previously reported for, e.g., kappa opioid receptor antagonist [^{11}C]LY2795050 or dopamine D2/D3 receptor agonist [^{11}C]PHNO, using similar equipment and techniques.[31,32] Correction of V_T for f_p can be considered as the "gold standard" V_T value, and could be reliably performed for [^{11}C]UCB-J as the measurement of f_p was very reproducible. There was a statistically significant linear correlation between f_p and V_T in 5 of the 15 examined brain regions (Supplemental Table 6), e.g. frontal cortex in supplemental Figure 8. Correction for f_p worsened the TRV and aTRV, and even more the ICC. There was variability of ICC across regions, which was likely related to the small number of volunteers and relatively low within-subject variability in this healthy control group. Use of ICC as a measure of reliability will be more important in a patient population, where intersubject variability reflects the heterogeneity of the disease. In summary, V_T values were highly reproducible and correction for f_p may be considered only when performing cross-sectional studies, especially if there are potential group or treatment differences in this value. The very low intersubject variability also implies that SV2A is highly conserved in healthy subjects.

V_T values from the parametric maps were very similar, and had comparable reproducibility to the TAC-based analysis. The V_T maps were of high quality, required no post-smoothing, and should enable high quality measurements in small brain regions, which is of high relevance for identifying small regional lesions in epilepsy or localized synaptic loss in neurodegenerative disorders. Alternatively, a substantially reduced radioactivity dose should produce acceptable parametric maps, albeit with some post-smoothing.

Evaluation of the time-stability of V_T indicated that the PET scan duration could be feasibly shortened to 60 min. It can be anticipated that in most diseases with loss of synapses, the V_T values will generally be lower and that less time will be required to approach equilibrium conditions. However, K_1 values, sensitive to blood flow, may be lower as well, and thereby extend the time to equilibrium in the diseased brain. It is thus important to re-evaluate this time-stability in disease-specific patient groups.

The main advantage of dynamic PET scans, including arterial blood sampling, is the opportunity to perform full kinetic modeling and determine individual rate parameters. One such important parameter is K_1, which is indicative of cerebral blood flow. Parametric K_1 maps of [^{11}C]UCB-J were also of high quality and provided nearly identical values to the TAC based method. Regional changes in K_1 can thus be examined on the parametric maps but with caution for the biased hippocampal region and can provide critical flow information for neurodegenerative diseases, in a similar approach as previously shown for [^{11}C]PIB.[33]

An alternative methodology for obtaining V_T values is the use of a bolus plus constant infusion approach.[23] During equilibrium conditions, arterial plasma concentrations may equilibrate with venous plasma concentrations and venous samples may then suffice for quantification of radioligand concentration in plasma, as recently validated for mGluR5 radioligand [^{18}F]FPEB.[34] When validated, the bolus plus constant infusion approach may thus allow for determination of V_T values without arterial cannulation, and potentially, with an even shorter scan.

An alternative approach to make arterial cannulation redundant is the use of a reference tissue model. Previous experiments in nonhuman primates demonstrated that the SV2A density was negligible in the centrum semiovale.[23] Using the centrum semiovale as a reference region in the current study, regional BP_{ND} values ($V_{T\ ROI}/V_{T\ centrum\ semiovale} - 1$) ranged between 3.26 ± 0.32 in the putamen and 1.67 ± 0.36 in the posterior cingulate cortex, with a regional mean aTRV of $5.3 \pm 4.1\%$. Further validation studies with SV2A selective inhibitors, e.g. levetiracetam or brivaracetam, are required to confirm the promise of a reference region approach for [^{11}C]UCB-J.

Funding

The author(s) disclosed receipt of the following financial support for the research, authorship, and/or publication of this article: Research support was provided by UCB Pharma. SJF

was supported by an International Postdoc grant from the Swedish Research Council. This publication was made possible by CTSA (grant no. UL1 TR000142) from the National Center for Advancing Translational Science (NCATS), a component of the National Institutes of Health (NIH). Its contents are solely the responsibility of the authors and do not necessarily represent the official view of NIH.

Acknowledgment

The authors thank the staff of the Yale PET Center for their expert assistance.

Declaration of conflicting interests

The author(s) declared the following potential conflicts of interest with respect to the research, authorship, and/or publication of this article: JM and JH were full-time employees of UCB Pharma at the time this work was planned, conducted, and analyzed. JH is currently a full-time employee of Denali Therapeutics. All other authors declare no competing financial interests.

Authors' contributions

SJF designed the study, performed the experiments, data analysis, and manuscript preparation; NBN performed the PET experiments; JM designed the study; S-fL performed metabolite analysis; M-KC performed the PET experiments; DM recruited subjects and performed the PET experiments; J-DG performed data analysis; SH recruited subjects and performed the PET experiments; JH designed the study; YH designed and performed the PET experiments; and REC designed the study, performed data analysis and manuscript preparation. All authors reviewed and approved the final version of this manuscript.

Supplementary material

Supplementary material for this paper can be found at the journal website: http://journals.sagepub.com/home/jcb

References

1. Mendoza-Torreblanca JG, Vanoye-Carlo A, Phillips-Farfan BV, et al. Synaptic vesicle protein 2A: basic facts and role in synaptic function. *Eur J Neurosci* 2013; 38: 3529–3539.
2. Nowack A, Yao J, Custer KL, et al. SV2 regulates neurotransmitter release via multiple mechanisms. *Am J Physiol Cell Physiol* 2010; 299: C960–C967.
3. Bajjalieh SM, Frantz GD, Weimann JM, et al. Differential expression of synaptic vesicle protein 2 (SV2) isoforms. *J Neurosci* 1994; 14: 5223–5235.
4. Janz R and Sudhof TC. SV2C is a synaptic vesicle protein with an unusually restricted localization: anatomy of a synaptic vesicle protein family. *Neuroscience* 1999; 94: 1279–1290.
5. van Vliet EA, Aronica E, Redeker S, et al. Decreased expression of synaptic vesicle protein 2A, the binding site for levetiracetam, during epileptogenesis and chronic epilepsy. *Epilepsia* 2009; 50: 422–433.
6. Feng G, Xiao F, Lu Y, et al. Down-regulation synaptic vesicle protein 2A in the anterior temporal neocortex of patients with intractable epilepsy. *J Mol Neurosci* 2009; 39: 354–359.
7. Lynch BA, Lambeng N, Nocka K, et al. The synaptic vesicle protein SV2A is the binding site for the antiepileptic drug levetiracetam. *Proc Natl Acad Sci U S A* 2004; 101: 9861–9866.
8. Goelz SE, Nestler EJ, Chehrazi B, et al. Distribution of protein I in mammalian brain as determined by a detergent-based radioimmunoassay. *Proc Natl Acad Sci U S A*. 1981; 78: 2130–2134.
9. De Camilli P, Harris SM Jr., Huttner WB, et al. Synapsin I (Protein I), a nerve terminal-specific phosphoprotein. II. Its specific association with synaptic vesicles demonstrated by immunocytochemistry in agarose-embedded synaptosomes. *J Cell Biol* 1983; 96: 1355–1373.
10. Masliah E, Terry RD, Alford M, et al. Quantitative immunohistochemistry of synaptophysin in human neocortex: an alternative method to estimate density of presynaptic terminals in paraffin sections. *J Histochem Cytochem* 1990; 38: 837–844.
11. Mutch SA, Kensel-Hammes P, Gadd JC, et al. Protein quantification at the single vesicle level reveals that a subset of synaptic vesicle proteins are trafficked with high precision. *J Neurosci* 2011; 31: 1461–1470.
12. Kaufman AC, Salazar SV, Haas LT, et al. Fyn inhibition rescues established memory and synapse loss in Alzheimer mice. *Ann Neurol* 2015; 77: 953–971.
13. Estrada S, Lubberink M, Thibblin A, et al. [^{11}C]UCB-A, a novel PET tracer for synaptic vesicle protein 2A. *Nucl Med Biol* 2016; 43: 325–332.
14. Nabulsi NB, Mercier J, Holden D, et al. Synthesis and preclinical evaluation of ^{11}C-UCB-J as a PET tracer for imaging the synaptic vesicle glycoprotein 2A in the brain. *J Nucl Med* 2016; 57: 777–784.
15. Cai H, Mangner TJ, Muzik O, Wang MW, et al. Radiosynthesis of ^{11}C-levetiracetam: a potential marker for PET imaging of SV2A expression. *ACS Med Chem Lett* 2014; 5: 1152–1155.
16. Bretin F, Warnock G, Bahri MA, et al. Preclinical radiation dosimetry for the novel SV2A radiotracer [^{18}F]UCB-H. *EJNMMI Res* 2013; 3: 35.
17. Gillard M, Chatelain P and Fuks B. Binding characteristics of levetiracetam to synaptic vesicle protein 2A (SV2A) in human brain and in CHO cells expressing the human recombinant protein. *Eur J Pharmacol* 2006; 536: 102–108.
18. Warnock GI, Aerts J, Bahri MA, et al. Evaluation of ^{18}F-UCB-H as a novel PET tracer for synaptic vesicle protein 2A in the brain. *J Nucl Med* 2014; 55: 1336–1341.
19. Bretin F, Bahri MA, Bernard C, et al. Biodistribution and radiation dosimetry for the novel SV2A radiotracer [^{18}F]UCB-H: first-in-human study. *Mol Imag Biol* 2015; 17: 557–564.
20. Zheng MQ, Holden D, Nabulsi N, et al. Synthesis and evaluation ^{18}F-UCB-H, a novel PET imaging tracer for the synaptic vesicle protein 2A. *J Nucl Med* 2014; 55: 1792.

21. Warnier C, Lemaire C, Becker G, et al. Enabling efficient positron emission tomography (PET) imaging of synaptic vesicle glycoprotein 2A (SV2A) with a robust and one-step radiosynthesis of a highly potent ^{18}F-labeled ligand ([^{18}F]UCB-H). *J Med Chem* 2016; 59: 8955–8966.
22. Nicolas JM, Hannestad J, Holden D, et al. Brivaracetam, a selective high-affinity synaptic vesicle protein 2A (SV2A) ligand with preclinical evidence of high brain permeability and fast onset of action. *Epilepsia* 2016; 57: 201–209.
23. Finnema SJ, Nabulsi NB, Eid T, et al. Imaging synaptic density in the living human brain. *Sci Transl Med* 2016; 8: 348ra96.
24. Carson RE, Barker WC, Liow JS, et al. Design of a motion-compensation OSEM list-mode algorithm for resolution-recovery reconstruction for the HRRT. *IEEE Nucl Sci Symp conf Rec* 2003; 5: 3281–3285.
25. Jin X, Mulnix T, Gallezot JD, et al. Evaluation of motion correction methods in human brain PET imaging – a simulation study based on human motion data. *Med Phys* 2013; 40: 102503.
26. Hilton J, Yokoi F, Dannals RF, et al. Column-switching HPLC for the analysis of plasma in PET imaging studies. *Nucl Med Biol* 2000; 27: 627–630.
27. Gallezot JD, Esterlis I, Bois F, et al. Evaluation of the sensitivity of the novel α4β2* nicotinic acetylcholine receptor PET radioligand ^{18}F-(-)-NCFHEB to increases synaptic acetylcholine levels in rhesus monkey. *Synapse* 2014; 68: 556–564.
28. Holmes CJ, Hoge R, Collins L, et al. Enhancement of MR images using registration for signal averaging. *J Comput Assist Tomogr* 1998; 22: 324–333.
29. Tzourio-Mazoyer N, Landeau B, Papathanassiou D, et al. Automated anatomical labeling of activations in SPM using a macroscopic anatomical parcellation of the MNI MRI single-subject brain. *Neuroimage* 2002; 15: 273–289.
30. Pajevic S, Daube-Witherspoon ME, Bacharach SL, et al. Noise characteristics of 3-D and 2-D PET images. *IEEE Transact Med Imag* 1998; 17: 9–23.
31. Naganawa M, Zheng MQ, Henry S, et al. Test–retest reproducibility of binding parameters in humans with ^{11}C-LY2795050, an antagonist PET radiotracer for the kappa opioid receptor. *J Nucl Med* 2015; 56: 243–248.
32. Gallezot JD, Zheng MQ, Lim K, et al. Parametric imaging and test–retest variability of ^{11}C-(+)-PHNO binding to D_2/D_3 dopamine receptors in humans on the high-resolution research tomograph PET scanner. *J Nucl Med* 2014; 55: 960–966.
33. van Berckel BN, Ossenkoppele R, Tolboom N, et al. Longitudinal amyloid imaging using ^{11}C-PiB: methodologic considerations. *J Nucl Med* 2013; 54: 1570–1576.
34. Park E, Sullivan JM, Planeta B, et al. Test–retest reproducibility of the metabotropic glutamate receptor 5 ligand [^{18}F]FPEB with bolus plus constant infusion in humans. *Eur J Nucl Med Mol Imag* 2015; 42: 1530–1541.